Supporting Information

Kürten et al. 10.1073/pnas.1404853111

SI Text

CLOUD Chamber and Instruments. The Cosmics Leaving Outdoor Droplets (CLOUD) experiment is designed to study the formation and growth of aerosol particles and the role of ions in these processes. Experiments were conducted at the CLOUD chamber in October 2012 for the ternary system involving sulfuric acid (SA), dimethylamine (DMA), and water vapor. The CLOUD experiment and the chamber have been described in previous publications (1, 2). A summary is given here that focuses on the aspects that are relevant for this study. The chamber consists of an electropolished stainless steel cylinder with a volume of 26.1 m^3. The neutral nucleation pathway can be studied when a high-voltage clearing field is enabled. This is achieved by applying +30 kV to an upper and −30 kV to a lower transparent field cage electrode. Ceramic spacers insulate the chamber from the electrodes, and the strong electric field sweeps out all ions produced by natural galactic cosmic rays within about 1 s. Ion-induced nucleation (IIN) is studied when the electrodes are grounded. In this case, natural galactic cosmic rays generate ions, which have been shown to enhance the new particle formation (NPF) rates for the binary sulfuric acid–water (H_2SO_4–H_2O) system as well as for the ternary system involving ammonia (NH_3) (1). For the ternary system with dimethylamine [$(CH_3)_2NH$], the ion-induced contribution is only important when sulfuric acid concentrations are low (2). Higher ionization rates are achieved by illuminating the chamber with a defocused charged pion beam from the European Organization for Nuclear Research (CERN) Proton Synchrotron. Ionization rates up to about 75 ion pairs·cm^{-3}·s^{-1} can be reached. From the perspective of the neutral cluster detection it is necessary to distinguish between the neutral and the IIN case. During IIN studies it has been observed that charged clusters from the chamber can contribute to the product ion signals originating from the neutral clusters measured with the Chemical Ionization–Atmospheric Pressure interface–Time Of Flight (CI-APi-TOF) mass spectrometers. Although the number concentration of the charged clusters is much lower than for the neutral clusters, the charged clusters can still contribute to the total ion signal because only a small fraction of the neutral species is ionized within the CI-APi-TOF drift tube. Therefore, the CI-APi-TOF-U-FRA (instrument from the University of Frankfurt) employs an ion precipitator integrated in its sampling line to remove the chamber ions. The CI-APi-TOF-U-HEL (instrument from the University of Helsinki) was not equipped with an ion precipitator; therefore, the data shown for this instrument are limited to the neutral runs.

The CLOUD chamber has been designed to achieve a very high level of cleanliness by avoiding contact between plastic materials and the gas inside the chamber. Nitrogen and oxygen from cryogenic liquids, which should be free of contaminants, are used. Minimizing contaminants to the extent possible is necessary when nucleation studies are performed at atmospherically relevant sulfuric acid concentrations, between about 1×10^6 and 1×10^7 cm^{-3}, because contamination with amines at similar levels can substantially enhance the new particle formation rate (2). Therefore, it is necessary to monitor the contents of the chamber for such species. An ion chromatograph is used to determine the mixing ratio of dimethylamine and ammonia (3). The Proton-Transfer Reaction Time of Flight Mass Spectrometer (4) primarily monitors the concentrations of organic compounds (5), but it can also be used for the measurement of ammonia (6) or dimethylamine. The APi-TOF mass spectrometer identifies the molecular compositions of ions and cluster ions (7). The mass spectrometer is identical to the one that is also used in the CI-APi-TOFs and is described in the next section. The APi-TOF does not include a charging unit; therefore, it provides meaningful data only during experimental runs when ions are present. The presence of ammonia or amines associated with sulfuric acid clusters during a NPF event points to contamination in case these substances were not added intentionally. This is a very direct way of identifying compounds that are nucleating. At a temperature of 278 K, contaminant ammonia is present and can be detected in the APi-TOF mass spectra (1), but dimethylamine has not been detected during CLOUD7 when it was not added to the chamber. When present at sufficiently high concentrations, DMA will rapidly displace ammonia in the clusters as has been shown in previous experimental and theoretical studies (8, 9). The mass defect plot (Fig. 1*A*) shows that only minor amounts of NH_3 are present in the large clusters (heptamer and larger). Therefore, the data shown here are valid for the ternary system including only sulfuric acid, water and dimethylamine.

In addition to the two CI-APi-TOFs that are used to measure the sulfuric acid monomer and cluster concentrations (see next section), the Chemical Ionization Mass Spectrometer (CIMS) is used to determine the sulfuric acid monomer concentration (10–12).

Sulfuric acid production is initiated by UV light that is brought into the chamber through a fiber-optic system (13). Photolysis of ozone and subsequent reactions with water vapor, sulfur dioxide, and oxygen will generate sulfuric acid. When the H_2SO_4 loss rate equals its production rate, the concentration reaches a steady state. Depending on the UV light intensity and the trace gas mixing ratios, the concentration can be controlled. The gas is homogenously mixed by two fans installed inside the chamber (14). Although the sulfuric acid is produced in situ, dimethylamine is taken from a gas bottle. Before it is introduced into the chamber, it is diluted with clean air to achieve the desired mixing ratios. The addition of the diluted dimethylamine is performed close to the lower mixing fan, which ensures its rapid distribution throughout the chamber. The reported dimethylamine mixing ratios are from the IC measurement (2, 3).

CI-APi-TOF Instruments. The CI-APi-TOF technique has recently been described by Jokinen et al. (15). A schematic drawing of the CI-APi-TOF-U-FRA is shown in Fig. S1. Within the ion source, a corona discharge is used to initiate the formation of $NO_3^-(HNO_3)_n$ (usually $n \leq 2$) primary ions from nitric acid that is added to the sheath gas. The ion source and ion drift tube are an exact copy of the ion source used in the CIMS and have been described in detail by Kürten et al. (12).

The sample flow rate into the instrument is defined by the difference between the flow rates that are taken from the ion source and the drift tube, i.e., the excess air and the flow that enters the mass spectrometer through a small pinhole, and the flows that are actively introduced, i.e., the sheath gas (clean gas + HNO_3) and a flow of dry nitrogen in front of the pinhole. The sample flow rate is ∼8.5 standard liters per minute. It enters the ion drift tube where it is surrounded concentrically by the sheath gas. The primary ions are directed toward the center of the sample flow by means of an electrostatic field so that they can interact with sulfuric acid monomers and clusters. These compounds can be ionized through proton-transfer reaction. The reaction scheme for the sulfuric acid monomer is

$$H_2SO_4 + NO_3^-(HNO_3)_n \rightarrow HSO_4^-(HNO_3)_{n-m+1} + m \cdot (HNO_3). \quad \textbf{[R1]}$$

The trajectory of the ions is defined by the geometry, flow field, and applied electrostatic voltages. Because the trajectories of the

primary ions and, therefore, the effective reaction time are not known, it is necessary to calibrate the instrument with a known amount of sulfuric acid in the sample flow (16). The quantification of the sulfuric acid monomer and clusters is described in the next section. Primary and product ions enter the vacuum chamber through a small pinhole (~350 μm in diameter).

The mass spectrometer (Tofwerk AG) includes the electronics for the data acquisition as well as the software for controlling the instrument and recording the mass spectra. The vacuum chamber is separated into four chambers that are differentially pumped. The pressure in the first stage is ~3 hPa, which is maintained by a scroll pump (TriScroll 600; Agilent Technologies). A quadrupole mass filter (Quad1) is used as ion guide and helps to transfer the ions to the next chamber. The second chamber contains another quadrupole ion guide (Quad2) and is connected to the first stage of a three-stage turbo pump. The third stage contains a lens stack that is used to focus the ions and to prepare them energetically before they reach the final stage consisting of the time-of-flight mass spectrometer. These last two stages are also connected to the three-stage turbo pump. The pressure in the time-of-flight chamber is $\sim 1 \times 10^{-6}$ hPa. A high-voltage pulse is used to deflect the ions and accelerate them toward a reflectron. The mass spectrometer can either be operated using just one reflectron (so-called V-mode due to the shape of the ion trajectories), or a second reflectron can be used to increase the mass resolving power through a longer flight path (so-called W-mode). Because the high mass resolving power can only be achieved at the expense of a reduced sensitivity, the V-mode was used throughout this study for both CI-APi-TOFs. Detection of the ions is achieved with a multichannel plate detector. The vacuum chamber part is also used in the APi-TOF mass spectrometer, which has been described in detail by Junninen et al. (7). Typically, preaveraged mass spectra are recorded with a time resolution of 5 s. For the evaluation of the time-of flight mass spectra the MATLAB-based Toftools software is used (7). The CI-APi-TOFs usually achieve a mass accuracy of better than 10 ppm and a mass resolving power up to 4,500 Th/Th.

The CI-APi-TOF-U-HEL and the CI-APi-TOF-U-FRA differ in certain aspects from each other. Although the originally developed CI-APi-TOF-U-HEL instrument used a radioactive ^{241}Am ion source, this source could not be used during the CLOUD experiment due to CERN's strict safety regulations. Therefore, an alternative method was deployed which makes use of a soft X-ray source (soft X-ray tube, N7599; Hamamatsu Photonics K.K.). The X-ray source is located outside of the ion source flange; the radiation is transmitted into the annular gap (where the corona needle is located in the CI-APi-TOF-U-FRA instrument in Fig. S1) through a thin Teflon foil. The interaction of the soft X-rays with the HNO_3 containing sheath gas produces the nitrate primary ions. This method yields very clean spectra with a stable ion count rate. The two instruments also differ in their sample tube diameters, drift tube lengths, and inner diameters. The relatively large dimensions of the Helsinki instrument result in an effective reaction time of ~200 ms; that of the smaller Frankfurt instrument is on the order of 50 ms. The different reaction times are taken into account by calibrating each instrument individually.

The corona discharge was found to lead to a greater abundance of background peaks than did the X-ray source. Increasing the amount of HNO_3 added to the sheath gas reduced the intensities of these signals. For this reason the amount of HNO_3 used in the sheath gas of the CI-APi-TOF-U-FRA was higher than in the Helsinki instrument. Because the neutral nitric acid can also interact with the sample gas, the increased HNO_3 concentration produces more SA–DMA clusters associated with nitric acid. However, although the spectra of the two instruments differ somewhat in this aspect, they show qualitatively the same results. In addition, deriving the cluster concentrations by summing up all signals related to a certain number of sulfuric acid molecules contained in the clusters yields remarkably good agreement between the two instruments (Fig. 3). This indicates that clustering with nitrate does not significantly influence the cluster detection efficiency.

As mentioned above, the CI-APi-TOF-U-FRA uses an ion precipitator integrated in its sampling line. The ion precipitator consists of a small piece of 0.5-inch stainless steel tubing which has been cut into two halves in the direction of flow. Applying 2 kV on one side and ground potential on the other half effectively removes all ions from the sample flow during ion-induced nucleation experiments.

A flow of nitrogen is added in front of the pinhole of the Frankfurt instrument (Fig. S1). The same design is used in CIMS instruments for the measurement of the sulfuric acid concentration and has, therefore, been adopted also for the CI-APi-TOF-U-FRA. When the ions travel through the dry nitrogen, water molecules are effectively removed from the core ions (17). This simplifies the mass spectra by avoiding that signals corresponding to a cluster with a given amount of sulfuric acid molecules are distributed over many peaks due to different numbers of water molecules associated with the core ion. Moreover, the nitrogen counterflow prevents the entry of fine particles and nitric acid into the vacuum chamber. The CI-APi-TOF-U-HEL does not use the N_2 counterflow.

Fragmentation of clusters as they transit from ambient pressure into the ultrahigh vacuum of the mass spectrometer cannot be ruled out (2, 18). This most likely happens in the Quad1 region where ion acceleration leads to energetic collisions with neutrals at relatively high pressure (several hPa). The extent of fragmentation is not known and needs to be further investigated in future studies. For this study, it can be concluded, however, that any fragmentation should affect mainly the trimer and the larger clusters. The agreement between modeled and measured dimer concentration is quite good (Figs. 2 and 3); moreover, the binding energy of the dimer ion $[HSO_4^-(H_2SO_4)]$ is very high, which should prevent its fragmentation when the CI-APi-TOFs are tuned to maximize the ratio between $HSO_4^-(HNO_3)$ and HSO_4^- (19). If a large fraction of the sulfuric acid monomer is detected as $HSO_4^-(HNO_3)$, the dimer should not fragment substantially because the binding energy of $HSO_4^-(HNO_3)$ (27.4 kcal·mole^{-1}) is considerably lower than for $HSO_4^-(H_2SO_4)$ (41.8 kcal·mole^{-1}) (20, 21). Fragmentation of clusters larger than the dimer could be occurring to some extent. This does, however, not change the interpretation from Fig. 3 that NPF is very likely proceeding at the kinetic limit. Fragmentation should reduce all measured cluster concentrations at a certain size by a constant factor. Because the slope of N_{cluster} vs. N_1 agrees best with the model calculations assuming zero evaporation, it can be concluded that the reduction in the cluster concentrations for N_3 and the larger clusters compared with the modeled concentrations are not due to evaporation of the neutral clusters.

Cluster Quantification. The sulfuric acid monomer concentration is estimated to be

$$[H_2SO_4] = N_1 = \frac{C_1}{T_1} \cdot \frac{S_{97} + S_{160}}{S_{62} + S_{125} + S_{188}}; \qquad \textbf{[S1]}$$

that is, it is proportional to the sum of the product ion signals S_{97} (m/z 97, HSO_4^-) and S_{160} [m/z 160, $HSO_4^-(HNO_3)$] divided by the sum of the primary ion signals S_{62} (m/z 62, NO_3^-), S_{125} [m/z 125, $NO_3^-(HNO_3)$], and S_{188} [m/z 188, $NO_3^-(HNO_3)_2$]. The constant C_1 is derived from calibration of the CI-APi-TOFs, during which a known concentration of H_2SO_4 is generated and from the measured signals the calibration constant is derived by the method described in ref. 16. The transmission efficiency of the sulfuric acid monomer through the sampling line from the CLOUD chamber to the ion drift tube of the CI-APi-TOFs is taken into account by the factor T_1. For straight circular tubes and laminar flow the transmission can be calculated from empirical equations (22). However, the two CI-APi-TOFs were connected to the

CLOUD chamber with one common sampling line which was split after a certain distance connecting each instrument to one arm of the y-splitter. For this geometry the transmission cannot be calculated with empirical equations. Therefore, the transmission efficiency was derived from comparison of the measured sulfuric acid monomer concentration with the CIMS (see above). This instrument has its own sampling line which consists of a straight tube and the CIMS was calibrated individually with the same calibration system as the CI-APi-TOFs. The transmission efficiency T_1 that has been derived from this method has a value of 0.32.

The evaluation of the cluster concentrations is more difficult because it is not yet possible to calibrate for these species. Generally, their concentrations can be derived from the following formula:

$$N_i = \frac{C_1}{T_1}\cdot\frac{k_1}{k_i}\cdot\frac{T_1}{T_i}\cdot\frac{e_1}{e_i}\cdot\frac{\sum \text{product ion signals}}{S_{62}+S_{125}+S_{188}}. \qquad \textbf{[S2]}$$

This equation takes into account three effects which lead to differences from the monomer. The first effect (term k_1/k_i) is the different reaction rate between the cluster and the primary ions compared with the monomer. Therefore, the equation needs to be scaled with the monomer reaction rate divided by the cluster reaction rate. The values for the monomer and the clusters are 1.9×10^{-9} $cm^3 \cdot s^{-1}$ (k_1 and k_2) and 2.2×10^{-9} $cm^3 \cdot s^{-1}$ (k_3 to k_5) [k_1 to k_4 from Chen et al. (19); k_5 tentatively set to the same value as k_4]. It should be noted that these rate constants are derived for pure sulfuric acid clusters. The presence of DMA in the clusters will likely change the ionization efficiencies depending on the amount of DMA. Currently, it is, however, not possible to calibrate for this effect. Therefore, the above values are being used.

The second correction term T_1/T_i accounts for the increase in the transmission efficiency through the sampling line with increasing size of the molecule or cluster due to its smaller diffusivity. This effect has been quantified by deriving an effective length for the known monomer transmission efficiency (23). Because this efficiency is known as a function of the flow rate and the diffusivity of the monomer, the length for which the experimentally determined monomer transmission efficiency would result can be calculated. With this information the transmission T_i for the clusters can be calculated with the equations provided in ref. 22.

The third term, e_1/e_i, considers mass discrimination effects from the acceptance of the pinhole, the quadrupole ion guides (Quad1 and Quad2), the time-of-flight mass spectrometer, and the multichannel plate detector. The relevant mass range of the product ions spans 97 Th (HSO_4^- ion) to 776 Th [$HSO_4^-(H_2SO_4)_4((CH_3)_2NH)_5(HNO_3)$ ion], and therefore, differences in the detection efficiency between light and heavy ions can be expected. However, it is not trivial to quantify this effect. This was attempted by calibration experiments where ions were generated by electrospray. Subsequently, ions within a narrow mobility range were selected with a high-resolution differential mobility analyzer (24). The flow from the high-resolution differential mobility analyzer was split, and one part was fed into an electrometer, whereas the other one was used as the sample flow for the CI-APi-TOF. The ratio of the signals obtained from the CI-APi-TOF and the electrometer for different ionic species covering a wide range of m/z values allows us to derive a relative transmission efficiency curve for the CI-APi-TOF. This is possible because the electrometer has a detection efficiency that is effectively independent of the ion mass if multiple charges can be ruled out. However, the resulting transmission curve cannot be directly applied to neutral clusters, because a fraction of the ions is precipitated in the sampling line before they can enter the drift tube during this calibration procedure. The negative ions experience a repulsing electric field just before they are transferred from the sampling line into the drift tube and are, therefore, accelerated toward the walls of the sampling line. This effect depends strongly on the ion mobility and, therefore, affects the small ions to a larger extent than the heavier ions.

For this reason, no corrections according to the obtained transmission curves were applied. Instead, a different method was used to verify that the monomer and dimer concentrations show similar transmission efficiencies. During the CI-APi-TOF calibration, high sulfuric acid monomer concentrations were generated. Under the clean conditions during a calibration, the neutral dimer concentration is negligible. Therefore, if the signal at m/z 195 [$HSO_4^-(H_2SO_4)$] is elevated, it is due to ion clustering between HSO_4^- product ions and H_2SO_4 within the CI-APi-TOF drift tube (25). The expected m/z 195 signal due to this process is (26)

$$S_{195} = \frac{1}{2\cdot C_1^2}\cdot[H_2SO_4]^2\cdot(S_{62}+S_{125}+S_{188}). \qquad \textbf{[S3]}$$

Here $[H_2SO_4]$ is the applied sulfuric acid monomer concentration and C_1 is the calibration constant for the monomers. Good agreement between the expected and the measured S_{195} indicates that the detection efficiency for the monomer and the dimer is very similar. Therefore, although the exact quantification of the trimer and larger clusters is not possible at the moment, the dimer concentration can be reported with a higher confidence. It should be noted that the above discussion (and also Eq. **S2**) leaves out the effect of potential cluster fragmentation.

Note that little ion clustering occurs in the CI drift tube during the NPF experiments because the sulfuric acid concentration is low enough (and the reaction/residence time is short enough) to prevent this effect.

Kinetic Model. The kinetic model that is used to calculate the cluster distributions is based on ref. 27. The time-dependent balance equation for the monomer concentration N_1 is

$$\frac{dN_1}{dt} = P_1 - \left(k_{1,w} + k_{dil} + \sum_{j=1}^{N} G_{1,j}\cdot\beta_{1,j}\cdot N_j\right)\cdot N_1 + 2\cdot k_{2,evap}\cdot N_2. \qquad \textbf{[S4]}$$

For the dimer the time-dependent concentrations can be calculated by

$$\frac{dN_2}{dt} = \frac{1}{2}\cdot G_{1,1}\cdot\beta_{1,1}\cdot N_1\cdot N_1 - \left(k_{2,w} + k_{dil} + \sum_{j=1}^{N} G_{2,j}\cdot\beta_{2,j}\cdot N_j\right)\cdot N_2 - k_{2,evap}\cdot N_2, \qquad \textbf{[S5]}$$

whereas for all larger clusters ($k > 2$),

$$\frac{dN_k}{dt} = \frac{1}{2}\cdot\sum_{i+j=k} G_{i,j}\cdot\beta_{i,j}\cdot N_i\cdot N_j - \left(k_{k,w} + k_{dil} + \sum_{j=1}^{N} G_{k,j}\cdot\beta_{k,j}\cdot N_j\right)\cdot N_k. \qquad \textbf{[S6]}$$

Here P_1 is the production rate of the monomers due to the generation of OH after the photolysis of ozone and subsequent reactions with water vapor, sulfur dioxide, and oxygen. The model of McMurry (27) has been extended to include the dimer evaporation rate ($k_{2,evap}$). All larger clusters are assumed to be stable. The loss terms in Eqs. **S4**–**S6** include the wall loss rate $k_{k,w}$ and the dilution rate k_{dil} that results from replenishment of the gas sampled by the instruments with clean gas. The dilution rate k_{dil} equals 9.6×10^{-5} s^{-1} and is determined by the ratio of the clean gas flow rate into the chamber (150 standard liters per minute) and the chamber volume (26.1 m^3). This factor is independent of

the cluster size, whereas the wall loss rate depends on the diffusivity of the molecule or cluster (28, 29):

$$k_{k,w} = C_w \cdot \sqrt{D_k}. \quad \text{[S7]}$$

The prefactor C_w has been estimated from experiments in which the decrease in the sulfuric acid or particle concentration has been observed as a function of time, $C_w = 0.0077\ \text{cm}^{-1}\cdot\text{s}^{-0.5}$. The diffusivity is calculated as function of the molecular weight of the cluster, temperature, and pressure. The third loss term describes the depletion of monomers due to self-coagulation and coagulation with larger clusters. The coagulation coefficient β is derived from kinetic theory (30),

$$\beta_{k,j} = \left(\frac{3}{4\pi}\right)^{1/6} \cdot \sqrt{\left(\frac{6k_bT}{m_k} + \frac{6k_bT}{m_j}\right)} \cdot \left(V_k^{1/3} + V_j^{1/3}\right)^2. \quad \text{[S8]}$$

It depends on the temperature T, the masses m_k and m_j of the clusters k and j, and their respective volumes V_k and V_j; k_b is the Boltzmann constant. The factor $G_{k,j}$ expresses the enhancement in the collision rates due to London–van der Waals forces and can be calculated from the formulas and the Hamaker constant given in ref. 31. The evaluated factors $G_{i,j}$ are around 2.3 for the free molecule regime, which is close to the value reported for nanometer-sized ammonium sulfate particles (32).

For simplicity it has been assumed that the clusters k are of the form $(H_2SO_4)_k((CH_3)_2NH)_k$. This means that when the concentration of dimethylamine in the presence of sulfuric acid is sufficiently high, all sulfuric acid is associated with DMA. This assumption is in accordance with quantum chemical calculations which suggest that clusters containing equal amounts of SA and DMA have very low evaporation rates (2, 30, 33, 34). Nevertheless, these calculations show that the evaporation rate of the smallest SA•DMA clusters is still nonnegligible. However, if the DMA concentration is large enough, the SA•DMA clusters form rapidly, and their fraction is large compared with the overall sulfuric acid concentration (sum of the free SA molecules and the SA•DMA clusters) (2). In this respect, large enough means that the arrival rate of a DMA molecule on a sulfuric acid molecule is at least as fast as the evaporation rate of a SA•DMA cluster. Ortega et al. (30) report an evaporation rate of $5.9 \times 10^{-2}\ \text{s}^{-1}$. Using the DMA mixing ratios during the experiments (between 5 and 32 pptv, i.e., concentrations between 1.3×10^8 and $8.3 \times 10^8\ \text{cm}^{-3}$) and a collision rate $k_{\text{SA,DMA}}$ of $5 \times 10^{-10}\ \text{cm}^3\cdot\text{s}^{-1}$, the arrival rate of a DMA molecule on a SA molecule can be calculated to be between 6.5×10^{-2} and $0.42\ \text{s}^{-1}$. Because these values are larger than the evaporation rate, it is justified to treat SA•DMA clusters as a single molecule in the kinetic model. Because the evaporation rates were reported for a temperature of 298 K (30) and the experiments were conducted at 278 K in this study, the stated evaporation rate is an upper limit.

The volumes in Eq. **S8** require the knowledge of the cluster densities. The density of the clusters is determined as the weighted average of the liquid bulk densities of sulfuric acid ($1.84\ \text{g}\cdot\text{cm}^{-3}$) and dimethylamine ($0.67\ \text{g}\cdot\text{cm}^{-3}$). This yields a density of $1.47\ \text{g}\cdot\text{cm}^{-3}$. Fission, i.e., nonmonomer evaporation from neutral clusters, was predicted based on quantum chemical calculations, e.g., for the cluster containing four SA and four DMA molecules (30, 34). However, the tetramer fission rate of $5 \times 10^{-2}\ \text{s}^{-1}$ is rather low (34). From our experimental results it cannot be concluded whether the fission of neutral tetramers is indeed occurring. If this would be the case the fission rate would probably be even lower than reported; otherwise, the slope of N_4 vs. N_1 in Fig. 3*C* should be steeper.

For the time-dependent cluster concentration modeling (Fig. 2) the production term P_1 in Eq, **S4** is adjusted until the modeled steady-state monomer concentration N_1 matches the measured concentration. The model results shown in Fig. 3 are obtained by varying the monomer concentration over the range from 1×10^6 to $2 \times 10^7\ \text{cm}^{-3}$. For each model run the cluster concentrations are calculated until a steady-state is reached. For the results shown, clusters up to $k = 2{,}000$ (d_{mob} ~9 nm) are included. For the accuracy of the model results it is actually not necessary to include that many clusters because the loss rate due to coagulation with the very large clusters is generally negligible in comparison with wall loss and loss to the smallest clusters.

Calculation of Dimer Formation Rates. In steady-state the production rate (P_2) or formation rate of the dimers (J_{dimer}) equals their loss rate (L_2):

$$\frac{dN_2}{dt} = P_2 - L_2 = J_{\text{dimer}} - L_2 = 0.$$

Dimer formation rates from the CI-APi-TOFs in Fig. 4 were therefore determined from the overall loss rate (L_2) and the steady-state dimer concentration (N_2),

$$J_{\text{dimer}}(t) = N_2 \cdot \left(\overline{CS}_2 + k_{2,w} + k_{\text{dil}}\right). \quad \text{[S9]}$$

Here it is taken into account that the dimers are lost due to coagulation, wall loss, and dilution of the chamber gas. The coagulation sink of the dimer can be determined from

$$\overline{CS}_2 = \overline{CS}_{2,\text{CI-APi-TOF}} + \overline{CS}_{2,\text{PSM}} + \overline{CS}_{2,\text{SMPS}}. \quad \text{[S10]}$$

The contributions of the coagulation sink for different cluster/particle size ranges were calculated based on the measurements from three different instruments. The first term takes into account the coagulation of dimers due to self-coagulation and coagulation with clusters up to the pentamer,

$$\overline{CS}_{2,\text{CI-APi-TOF}} = \sum_{k=1}^{5} \left(G_{2,k} \cdot \beta_{2,k} \cdot N_k\right). \quad \text{[S11]}$$

The second term considers the loss of dimers on small particles. The number density of particles in the size range between 1.3 and 3 nm was measured by the particle size magnifier (PSM) (35), operating in scanning mode (36):

$$\overline{CS}_{2,\text{PSM}} = \sum_{k=d_{p,1}}^{d_{p,N}} \left(G_{2,k} \cdot \beta_{2,k} \cdot N_k\right). \quad \text{[S12]}$$

Loss on larger particles was taken into account by using the size distributions obtained with a scanning mobility particle sizer (SMPS) starting at diameters around 4 nm:

$$\overline{CS}_{2,\text{SMPS}} = \sum_{k=d_{p,1}}^{d_{p,N}} \left(G_{2,k} \cdot \beta_{2,k} \cdot N_k\right). \quad \text{[S13]}$$

The average of a time period of a nucleation run where the dimer formation rates reach a steady-state determines the reported J_{dimer} in Fig. 4.

Comparison Between Measured Data and Model Results. To find out which model curve from Fig. 3 best describes the measured data, the ratio of the measured and the modeled concentrations was calculated for all data according to

$$r_i\left(k_{2,\text{evap}}\right) = \frac{N_{i,\text{measured}}}{N_{i,\text{modeled}}\left(k_{2,\text{evap}}\right)}, \quad \text{[S14]}$$

where i = 2, 3, 4, and 5 and $k_{2,\mathrm{evap}}$ is either 0, 10^{-2}, or 10^{-1} s^{-1}. The results for zero dimer evaporation are shown in Fig. S2. This figure shows the factor, which best describes the discrepancy between modeled and measured data. There is a clear trend that the larger clusters are detected with a lower efficiency. The main cause for this effect needs to be investigated in the future. It is, however, suspected that mass discrimination in the mass spectrometer and charging efficiency play the most important role.

The results taking into account different evaporation rates in the model and the CI-APi-TOF-U-FRA data are shown in Fig. S3. From this figure it is evident that the ratios calculated for $k_{2,\mathrm{evap}} = 0$ s^{-1} yield the most consistent values with the smallest scatter (SD). This supports the assumption that the deviation between measured and modeled data can be explained by a constant scaling factor, which arises from the uncertainties in the charging and the detection efficiencies of the clusters.

To test whether random variation can be responsible for the deviation from a constant ratio, statistical tests (f test) have been performed, which test the validity of the following zero hypotheses:

$$\text{a)}\quad \mathrm{Var}\left[r_i\left(k_{2,\mathrm{evap}}=0\right)\right] = \mathrm{Var}\left[r_i\left(k_{2,\mathrm{evap}}=10^{-2}\mathrm{s}^{-1}\right)\right] \qquad \textbf{[S15]}$$

and

$$\text{b)}\quad \mathrm{Var}\left[r_i\left(k_{2,\mathrm{evap}}=0\right)\right] = \mathrm{Var}\left[r_i\left(k_{2,\mathrm{evap}}=10^{-1}\mathrm{s}^{-1}\right)\right] \qquad \textbf{[S16]}$$

for each cluster i = 2, 3, 4, and 5. The f test yields a P value describing the probability to obtain the given samples if the zero hypothesis were correct. Therefore, low values indicate that it is quite improbable that the zero hypothesis is correct. The test results (P values) are given in the annotations of Fig. S3. For example, a value of 1.33×10^{-15} (Fig. S3*A*) indicates that the hypothesis "the variations in $r_2(k_{2,\mathrm{evap}} = 0\ s^{-1})$ are identical to the variations in $r_2(k_{2,\mathrm{evap}} = 10^{-2}\ s^{-1})$" is correct only with an extremely low probability of 1.33×10^{-15}. Testing for similarity between the SDs of $r_2(k_{2,\mathrm{evap}} = 0\ s^{-1})$ and $r_2(k_{2,\mathrm{evap}} = 10^{-1}\ s^{-1})$ yields a probability of zero. From this perspective it is very likely that the dimer evaporation rates are smaller than 10^{-2} s^{-1}. Performing the same analysis for the Helsinki data (CI-APi-TOF-U-HEL data from Fig. 3) yields the result that the dimer evaporation rates are smaller than 0.1 s^{-1}.

Further Evidence for Clusters Forming at the Kinetic Limit. Independent evidence that indicates absence of significant cluster evaporation is provided by the time development of the clusters at the start of the run. Fig. S4 shows cluster concentrations (N_1 to N_5) recorded during a nucleation experiment where the monomer concentration (N_1) reached a maximum value of 2.2×10^6 cm^{-3} during steady-state. Similarly, the cluster concentrations (N_2 to N_5) reached a constant value. Normalizing all cluster concentrations by their respective steady-state values yields the experimental data shown in Fig. S4. The same normalization was performed for the calculated cluster concentrations from the kinetic model (solid lines in Fig. S4). This allows the time development of the modeled and measured cluster concentrations to be compared without making any assumptions on the detection efficiency of the CI-APi-TOF mass spectrometer. Assuming an evaporation rate of zero for the dimer (Fig. S4*A* with $k_{2,\mathrm{evap}}$ = 0 s^{-1}) yields good agreement between measured and modeled appearance times of the clusters. Introducing finite evaporation rates of 0.01 s^{-1} or 0.1 s^{-1} (Fig. S4 *B* and *C*, respectively) predicts slower appearance times of the clusters that are incompatible with experimental measurements. The comparison between measured and modeled normalized cluster concentrations also reveals that the theoretical collision rates adequately describe the cluster dynamics.

1. Kirkby J, et al. (2011) Role of sulphuric acid, ammonia and galactic cosmic rays in atmospheric aerosol nucleation. *Nature* 476(7361):429–433.
2. Almeida J, et al. (2013) Molecular understanding of sulphuric acid-amine particle nucleation in the atmosphere. *Nature* 502(7471):359–363.
3. Praplan AP, Bianchi F, Dommen J, Baltensperger U (2012) Dimethylamine and ammonia measurements with ion chromatography during the CLOUD4 campaign. *Atmos Meas Tech* 5(9):2161–2167.
4. Graus M, Müller M, Hansel A (2010) High resolution PTR-TOF: Quantification and formula confirmation of VOC in real time. *J Am Soc Mass Spectrom* 21(6):1037–1044.
5. Schnitzhofer R, et al. (2013) Characterisation of organic contaminants in the CLOUD chamber at CERN. *Atmos Meas Tech Discuss* 6(4):7709–7734.
6. Norman M, Hansel A, Wisthaler A (2007) O_2^+ as reagent ion in the PTR-MS instrument: Detection of gas-phase ammonia. *Int J Mass Spectrom* 265(2–3):382–387.
7. Junninen H, et al. (2010) A high-resolution mass spectrometer to measure atmospheric ion composition. *Atmos Meas Tech* 3(4):1039–1053.
8. Bzdek BR, Ridge DP, Johnston MV (2010) Amine exchange into ammonium bisulfate and ammonium nitrate nuclei. *Atmos Chem Phys* 10(8):3495–3503.
9. Kupiainen O, Ortega IK, Kurtén T, Vehkamäki H (2012) Amine substitution into sulfuric acid – ammonia clusters. *Atmos Chem Phys* 12(8):3591–3599.
10. Eisele FL, Tanner DJ (1993) Measurement of the gas phase concentration of H_2SO_4 and methane sulfonic acid and estimates of H_2SO_4 production and loss in the atmosphere. *J Geophys Res* 98(D5):9001–9010.
11. Berresheim H, Elste T, Plass-Dülmer C, Eisele FL, Tanner DJ (2000) Chemical ionization mass spectrometer for long-term measurements of atmospheric OH and H_2SO_4. *Int J Mass Spectrom* 202(1–3):91–109.
12. Kürten A, Rondo L, Ehrhart S, Curtius J (2011) Performance of a corona ion source for measurement of sulfuric acid by chemical ionization mass spectrometry. *Atmos Meas Tech* 4(3):437–443.
13. Kupc A, et al. (2011) A fibre-optic UV system for H_2SO_4 production in aerosol chambers causing minimal thermal effects. *J Aerosol Sci* 42(8):532–543.
14. Voigtländer J, Duplissy J, Rondo L, Kürten A, Stratmann F (2012) Numerical simulations of mixing conditions and aerosol dynamics in the CERN CLOUD chamber. *Atmos Chem Phys* 12(4):2205–2214.
15. Jokinen T, et al. (2012) Atmospheric sulphuric acid and neutral cluster measurements using CI-APi-TOF. *Atmos Chem Phys* 12(9):4117–4125.
16. Kürten A, Rondo L, Ehrhart S, Curtius J (2012) Calibration of a chemical ionization mass spectrometer for the measurement of gaseous sulfuric acid. *J Phys Chem A* 116(24):6375–6386.
17. Zhao J, Eisele FL, Titcombe M, Kuang C, McMurry PH (2010) Chemical ionization mass spectrometric measurements of atmospheric neutral clusters using the cluster-CIMS. *J Geophys Res* 115(D8):D08205.
18. Olenius T, et al. (2013) Comparing simulated and experimental molecular cluster distributions. *Faraday Discuss* 165:75–89.
19. Chen M, et al. (2012) Acid-base chemical reaction model for nucleation rates in the polluted atmospheric boundary layer. *Proc Natl Acad Sci USA* 109(46): 18713–18718.
20. Curtius J, Froyd KD, Lovejoy ER (2001) Cluster ion thermal decomposition (I): Experimental kinetics study and ab initio calculations for $HSO_4^-(H_2SO_4)_x(HNO_3)_y$. *J Phys Chem A* 105(48):10867–10873.
21. Lovejoy ER, Curtius J (2001) Cluster ion thermal decomposition (II): Master equation modeling in the low-pressure limit and fall-off regions. Bond energies for $HSO_4^-(H_2SO_4)_x(HNO_3)_y$. *J Phys Chem A* 105(48):10874–10883.
22. Cheng YS (2001) *Condensation Detection and Diffusion Size Separation Techniques*, eds Baron PA, Willeke K (Wiley, New York).
23. Karlsson MNA, Martinsson BG (2003) Methods to measure and predict the transfer function size dependence of individual DMAs. *J Aerosol Sci* 34(5):603–625.
24. Steiner G, Attoui M, Wimmer D, Reischl GP (2010) A medium flow, high-resolution Vienna DMA running in recirculating mode. *Aerosol Sci Technol* 44(4):308–315.
25. Hanson DR, Eisele FL (2002) Measurement of prenucleation molecular clusters in the NH_3, H_2SO_4, H_2O system. *J Geophys Res* 107(D12):4158.
26. Hanson DR, Lovejoy ER (2006) Measurement of the thermodynamics of the hydrated dimer and trimer of sulfuric acid. *J Phys Chem A* 110(31):9525–9528.
27. McMurry PH (1980) Photochemical aerosol formation from SO_2: A theoretical analysis of smog chamber data. *J Colloid Interf* 78(2):513–527.
28. Crump JG, Seinfeld JH (1981) Turbulent deposition and gravitational sedimentation of an aerosol in a vessel of arbitrary shape. *J Aerosol Sci* 12(5):405–415.
29. Metzger A, et al. (2010) Evidence for the role of organics in aerosol particle formation under atmospheric conditions. *Proc Natl Acad Sci USA* 107(15):6646–6651.
30. Ortega IK, et al. (2012) From quantum chemical formation free energies to evaporation rates. *Atmos Chem Phys* 12(1):225–235.
31. Chan TW, Mozurkewich M (2001) Measurement of the coagulation rate constant for sulfuric acid particles as a function of particle size using tandem differential mobility analysis. *J Aerosol Sci* 32(3):321–339.
32. Brockmann JE, McMurry PH, Liu BYH (1982) Experimental study of simultaneous coagulation and diffusional loss of free molecule aerosols in turbulent pipe flow. *J Colloid Interface Sci* 88(2):522–529.
33. Kurtén T, Loukonen V, Vehkamäki H, Kulmala M (2008) Amines are likely to enhance neutral and ion-induced sulfuric acid-water nucleation in the atmosphere more effectively than ammonia. *Atmos Chem Phys* 8(14):4095–4103.
34. Ortega IK, et al. (2013) Corrigendum to "From quantum chemical formation free energies to evaporation rates" published in Atmos. Chem. Phys., 12, 225–235, 2012. *Atmos Chem Phys* 13(6):3321–3327.
35. Vanhanen J, et al. (2011) Particle size magnifier for nano-CN detection. *Aerosol Sci Technol* 45(4):533–542.
36. Wimmer D, et al. (2013) Performance of diethylene glycol-based particle counters in the sub-3nm size range. *Atmos Meas Tech* 6(7):1793–1804.

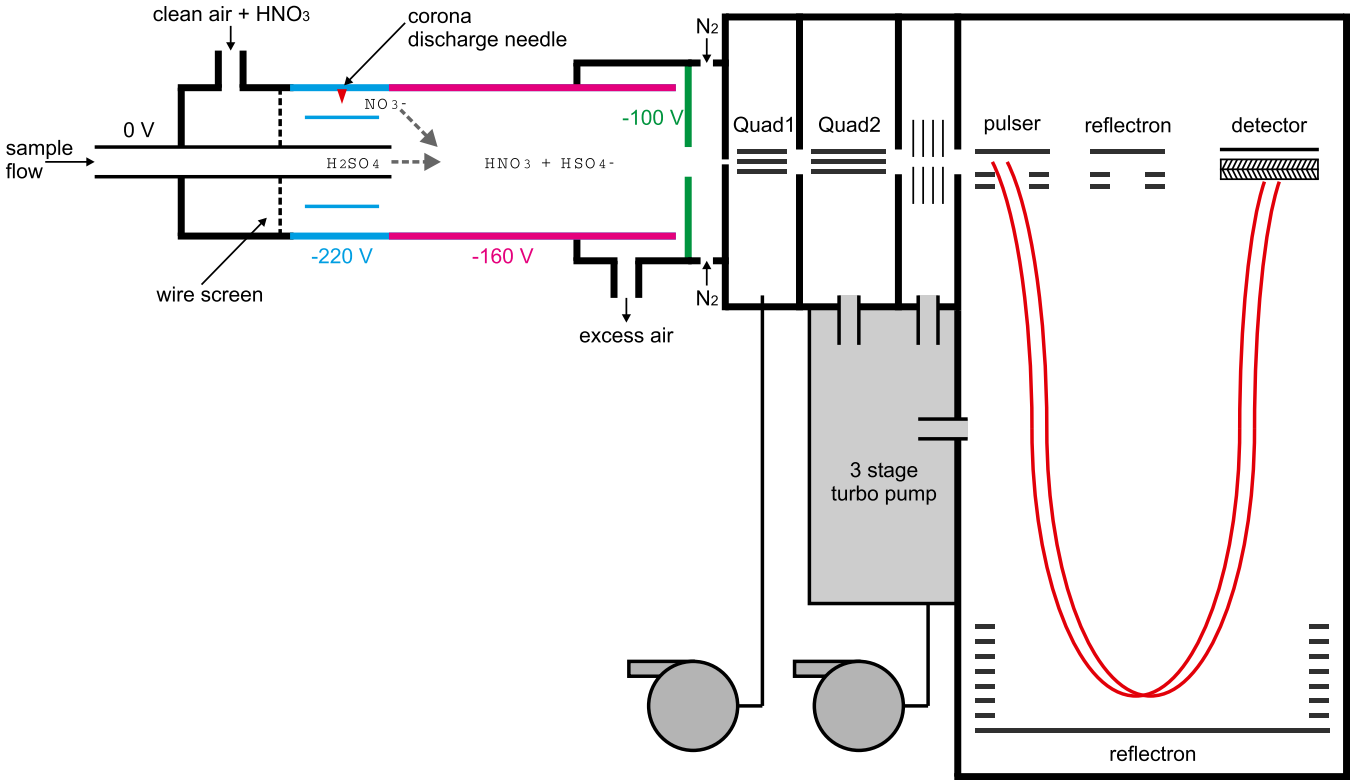

Fig. S1. Schematic drawing of the CI-APi-TOF mass spectrometer. Drawing is showing the instrument from the University of Frankfurt (CI-APi-TOF-U-FRA), which uses a corona discharge to generate the primary ions. The instrument from the University of Helsinki (CI-APi-TOF-U-HEL) uses a soft X-ray source for this task. The two instruments also differ in certain other details (*SI Text*). Drawing is not to scale.

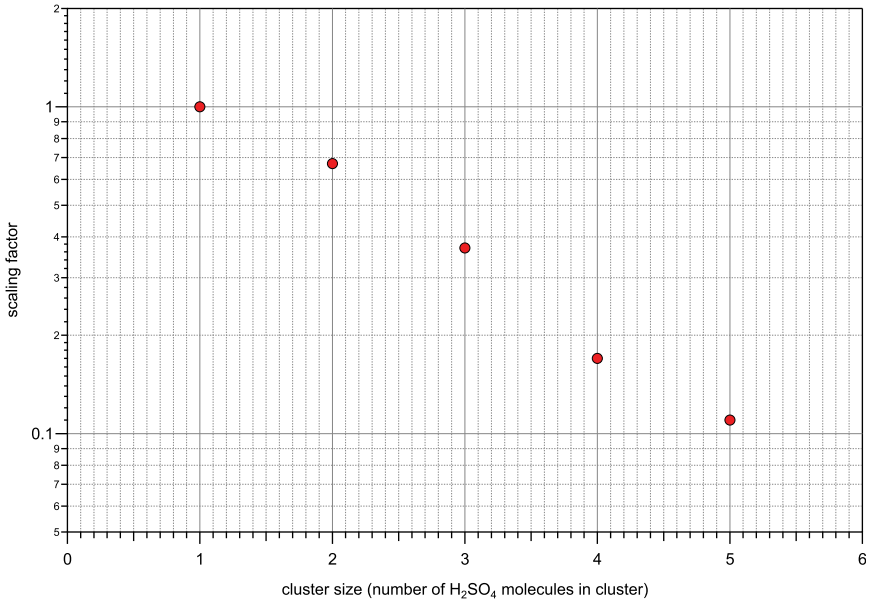

Fig. S2. Scaling factor for different cluster sizes. Scaling factor is derived by dividing the measured cluster concentrations by the modeled concentrations assuming zero dimer evaporation (Fig. 3). Qualitatively, the smooth decrease in the scaling factor is consistent with a decrease in the mass spectrometer sensitivity rather than with an increase in cluster evaporation rates.

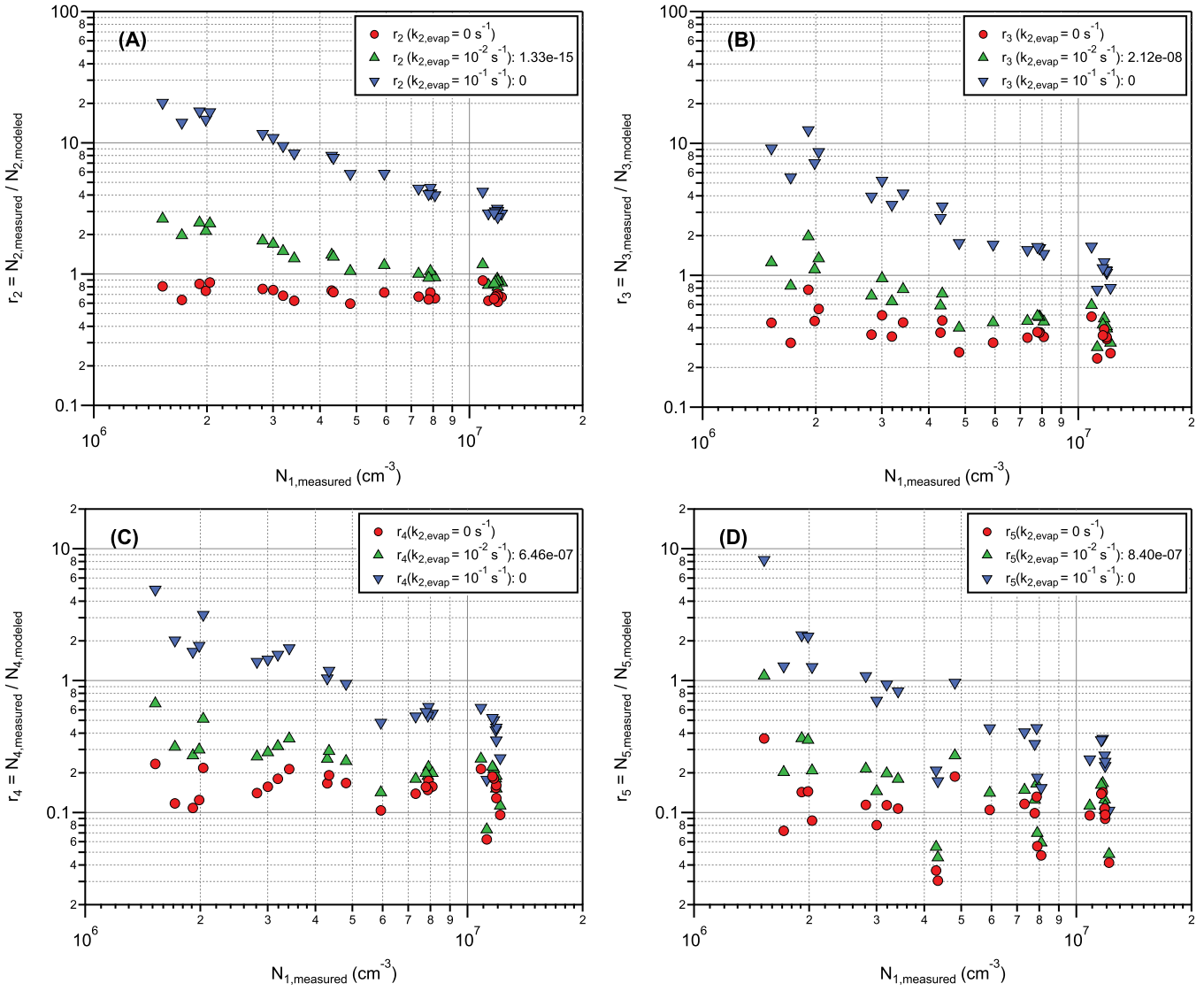

Fig. S3. Ratios between measured and calculated cluster concentrations as function of the sulfuric acid monomer concentration. Results are shown for (*A*) the dimer, (*B*) the trimer, (*C*) the tetramer, and (*D*) the pentamer for the measured data by the CI-APi-TOF mass spectrometer from the University of Frankfurt (CI-APi-TOF-U-FRA). Assuming different evaporation rates in the model, three different ratios were calculated for each cluster size. The numbers in the figure legend provide information about the similarity between the variance of the ratios assuming no dimer evaporation ($k_{2,evap} = 0\ s^{-1}$) and the variance of the ratios assuming nonzero dimer evaporation ($k_{2,evap} \geq 10^{-2}\ s^{-1}$). See *SI Text* for details.

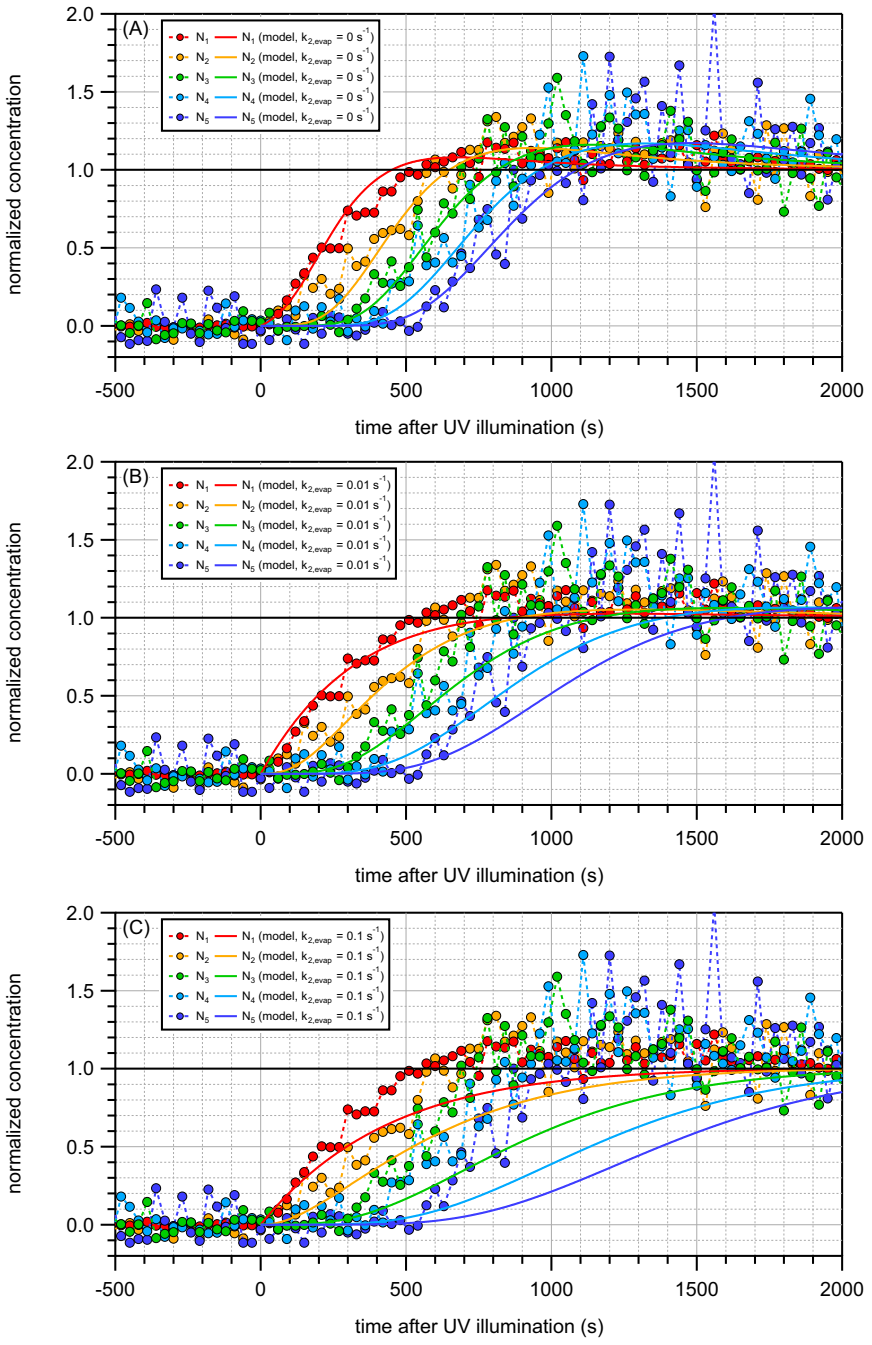

Fig. S4. Normalized cluster concentrations (N_1 to N_5) measured by the CI-APi-TOF ($N_1 = 2.2 \times 10^6$ cm^{-3}). Model calculations are shown by the solid lines assuming different dimer evaporation rates [$k_{2,evap} = 0$ s^{-1} (*A*), $k_{2,evap} = 0.01$ s^{-1} (*B*), and $k_{2,evap} = 0.1$ s^{-1} (*C*)].